JOM Journal of Optical Microsystems

RESEARCH PAPER

Impact of magnetic nanoparticles on the stability of blue phase and twist-grain boundary A phases

Apparao Gudimalla,[a,b,*] Marta Lavrič,[b] Brigita Rožič,[a,b] Saso Gyergyek,[c] Samo Kralj,[b,d] and Zdravko Kutnjak[a,b]

[a]Jožef Stefan International Postgraduate School, Ljubljana, Slovenia
[b]Jožef Stefan Institute, Condensed Matter Physics Department, Ljubljana, Slovenia
[c]Jožef Stefan Institute, Department of Materials Synthesis, Ljubljana, Slovenia
[d]University of Maribor, Faculty of Natural Sciences and Mathematics, Maribor, Slovenia

ABSTRACT. We investigate experimentally the impact of roughly spherular magnetic maghemite (γ-Fe_2O_3) nanoparticles (NPs) on the stabilization of lattices of topological line defects in liquid crystals (LCs). For this purpose, we exploit chiral CE8 LCs, which in bulk exhibit blue phases (BPs) possessing line defects (disclinations) in orientational order. Furthermore, the magnetic NPs stabilize twist-grain boundary A (TGB_A) and chiral line liquid (N_L^*) phase possessing screw line defects (dislocations) in translational order. Appropriately surface-decorated NPs stabilize these qualitatively different configurations of line defects owing to the defect core replacement and adaptive defect core targeting mechanisms. Magnetic NPs enhance the temperature window of BPI stability and stabilize TGB_A and N_L^* phases which are absent in bulk LC. Their impact is like the one imposed by strongly geometrically anisotropic NPs, which do not exhibit ferroelectric or ferromagnetic properties.

 [DOI: 10.1117/1.JOM.3.4.041206]

Keywords: liquid crystals; disclinations; dislocations; magnetic nanoparticles; phase stabilization

Paper 23013SS received Jun. 22, 2023; revised Sep. 4, 2023; accepted Sep. 7, 2023; published Oct. 10, 2023.

1 Introduction

Liquid crystal (LC) phases could host various topological defects (TDs).[1–3] Furthermore, LC phases exhibiting lattices of line defects could be exploited for various applications, particularly in photonics and other band-gap-based electro-optic applications.[4] These crystal-like defect lattice configurations could be efficiently manipulated by appropriate nanoparticles (NPs),[5] which provide a controllable pathway to stabilize or even structurally manipulate such defect assemblies.

LCs consist of anisotropic molecules whose ordering can be described at the mesoscopic scale by relevant order parameter fields.[1] In thermotropic uniaxial LCs consisting of rode-like molecules, which we consider in our research, orientational or, in addition, translational order exists in appropriate temperature windows. At high enough temperatures, such LCs display isotropic (I), an ordinary liquid phase where order parameter fields are melted. On lowering the temperature, LC order is established. Local uniaxial orientational order is commonly given by the nematic director field $\vec{n}$, where $\pm\vec{n}$ orientations are physically equivalent (the so-called head-to-tail invariance) and $|\vec{n}| = 1$. The nematic (N) uniaxial phase represents the simplest achiral LC phase. In bulk equilibrium, it exhibits long-range orientational order where $\vec{n}$ is spatially homogeneously aligned along a single symmetry-breaking directions. On further

*Address all correspondence to Apparao Gudimalla, appigspl@gmail.com; apparao.gudimalla@ijs.si

lowering temperature, smectic A (SmA) phase could be stabilized, which exhibits quasi-long-range translational order in addition to orientational order. The latter, in bulk equilibrium, consists of a parallel stack of smectic layers of periodicity d, where the layer normal points along $\vec{n}$. These structures do not exhibit line defects in bulk equilibrium.

One needs chiral LC molecules to stabilize lattices of line defects in LC configurations. In weakly chiral systems, the nematic phase is replaced by the chiral nematic (N^*), also referred to as the cholesteric phase.[1] This phase consists of cross-sections exhibiting nematic order uniformly twisted along the perpendicular direction. For a strong enough chirality, different blue phase (BP) configurations[6] could be introduced between the isotropic and N^* phases. These structures exhibit lattices of line defects (disclinations) in orientational order. Furthermore, twist-grain boundary A (TGB_A) and chiral line liquid (N_L^*) configurations[3,7] exhibiting lattices of screw line defects (dislocations) in translational order could intervene in a temperature window separating the defect-less N^* and SmA phases.

In the following, we summarize the main features of BP and TGB configurations. Reinitzer discovered LCs in 1888,[8] but the actual research interest in BPs started much later in the 1960s. BPs appear as a highly twisted nematic LC on cooling down from the isotropic phase. BPs are highly fluid self-assembled three-dimensional cubic structures formed by disclinations.[9] Three distinct BP phases can exist, which commonly appear in a narrow temperature interval 2-3 K between the I and the N^* phase.[2] The basic block of BPs consists of a so-called double-twist cylinder. Within it, chiral molecules exhibit "double-twist" deformation, which are energetically more favorable than a single twist[10–12] realized in N^*. These blocks tend to be arranged mutually perpendicularly, and due to topological reasons, a lattice of $m = -1/2$ disclinations needs to be introduced. Here m refers to the winding number,[1] reflecting the total reorientation of $\vec{n}$ by encircling counter-clockwise a line defect by any closed path. These defects form a cubic lattice, where the characteristic lattice linear scale is typically in the range of several hundred nm.[10] There are three different kinds of such phases: BPI, BPII, and BPIII.[13] BPI and BPII display a relatively high degree of translational order. BPI exhibits a cubic body-centered structure, while BPII has a simple cubic unit. On the other hand, in BPIII, a glass-type of disclination order is established.

Due to the narrow stability range, BPs have been of interest only for fundamental studies for a long time.[5,14,15] However, with time the scientific community realized the BPs potential for various applications in emerging technologies,[14] such as three-dimensional lasers, tunable photonic crystals, and fast optical displays.[4,16–18] This has initiated extensive research efforts in recent decades to increase their temperature stability range. Several strategies, such as chiral doping, polymer, and nanoparticles (NPs) stabilization, as well as long-timescale preservation in a supercooled state, were successfully exploited for the stabilization of BPs in wide temperature ranges.[10,15,19–35]

Furthermore, chirality favors twist-like configurations, which are incompatible with the smectic layer-type configurations. Consequently, for large enough chirality, lattices of screw disclinations could appear to energetically compromise the conflicting twist elastic deformations and smectic layer order. For example, the TGB_A phase consists of bulk-like SmA blocks, where the neighboring blocks are twisted for a finite angle. This twist is enabled by a lattice of screw dislocations that reside in the so-called grain boundaries. TGB_A was predicted based on de Gennes's mathematical analogy between smectic LCs and superconductors.[36] He claimed that both phases could be described with a complex order parameter. He demonstrated a complete analogy between the N–SmA and the normal metal-superconducting phase transition. By extending this analogy to structures possessing TDs, Renn and Lubensky[37] proposed the TGB_A configuration[38] as the LC analog to the Abrikosov flux phase appearing in type-II superconductor in the presence of an external magnetic field. Twist penetrates the TGB_A structure via a lattice of screw dislocations that are roughly analogs of magnetic vortices[3] in the type-II superconducting phase. In the latter case, an external magnetic field enforces the Abrikosov flux lattice.[39] Furthermore, the TGB phase could melt to a chiral line liquid just as the Abrikosov phase melts to a directed line liquid, as predicted by Kamien and Lubensky.[7] They predicted the existence of a short-range TGB structure corresponding to a liquid of screw dislocations. This phase is referred to as the chiral line liquid (N_L^*). Note that TGB and N_L^* are not thermodynamically distinct phases because they share the same phase symmetry. However, they differ in the range of translational order.[3]

Experimentally, Goodby et al. discovered the TGB phase in 1989.[37,40,41] The optical properties of this phase are similar to the N^* phase. Srajer et al.[42] showed that this phase's small-angle x-ray structure factor displays a continuous ring, which is consistent with the model of Renn and Lubensky. The existence of the lattice of screw dislocations was confirmed by the freeze-fracture measurements of Ihn et al.[43] The phase sequence $N^* - TGB_A - SmA$ was first detected by Lavrentovich et al.[44] Different TGB and N_L^* structures have been reported in Ref. 45.

Recent studies[28,46,47] show that appropriate surface-decorated NPs could be exploited to enhance the stability of LC structures exhibiting lattices of defects. The main stability generators are the defect core replacement (DCR)[28,46] and the adaptive defect core targeting (ADCT)[47] mechanisms. The DCR mechanism refers to the stabilization of defects via the partial replacement of energetically expensive TD cores volume with the volume of trapped NPs. The ADCT mechanism describes conditions necessary to efficiently target NPs to the cores of TDs. In recent studies, mostly the impact of particle size, geometry, and surface treatment on the stability of defect lattices have been carried out. These studies yield the following conclusions. Smaller NPs (of diameter below 100 nm) are more effectively trapped in the cores of TDs. Spherical NPs enhance the stability of BPIII configuration. On the other hand, nanoplatelets and nanosheets promote the stability of the BPI lattice structure. Note that the characteristic linear size of these 2D-like geometries is much larger than the defect core diameter. Consequently, only part of their volume could be immersed within the defect cores. There might stabilize lattice defects also by some other mechanism. Namely, their placement within defect lattices has not yet been directly experimentally probed. To promote capturing of NPs to defect cores, NPs should be adaptive to a local LC structure. Generally, this is achieved by decorating NP surfaces with long-enough flexible chains. In these studies, the impact of magnetic NPs on the stability of defect lattices has not been studied, and this is the focus of this paper.

The article is organized as follows. In Sec. 2, we describe the used materials and experimental details. Results of optical microscopy and high-resolution calorimetry are presented in Sec. 3. Results are discussed in Sec. 4. In the last section, conclusions are presented.

2 Materials and Methods

A strongly chiral LC compound S-(+)-[4-(2'-methyl butyl) phenyl 4'-n-octylbiphenyl-4-carboxylate] (CE8) has been purchased from Merck and used without further treatment. Magnetic NPs consisted of maghemite (γ-Fe_2O_3) with an average diameter of around 10 nm. The NPs were synthesized by co-precipitation of Fe(II) and Fe(III) cations with ammonia, followed by adsorption of oleic acid (OA).[48] The addition of HNO_3 flocculated the hydrophobized NPs. The particles were soaked in OA for coating, and the excess acid was removed by washing NPs with acetone. The composition of magnetic NPs was determined from selected area electron diffraction pattern and energy dispersive x-ray spectroscopy. The pattern was consistent with the cubic spinel structure, while the spectrum showed the presence of Fe and O elements. The average diameter d_{TEM} of NPs was estimated using TEM and DLS (Fig. 1) and was found to be $d_{TEM} = 10\ \text{nm} \pm 2\ \text{nm}$.

The protocol used to prepare CE8-magnetic NPs mixtures is described in Refs. 26 and 49–51. We studied NPs concentrations $\chi = 0.01$, 0.001, and 0.0001, where $\chi = m_{NP}/(m_{NP} + m_{LC})$. Here, m_{NP} and m_{LC} stand for the total masses of NPs and LC molecules in samples. After mixing, the mixtures were quenched immediately with cold water to keep the mixtures in the crystalline phase. These samples were then studied experimentally.

LC phase behaviour of mixtures was determined using optical microscopy and high-resolution calorimetry. The homemade extremely subtle temperature (± 0.01 K) controller attached to the optical microscopy was used to identify various LC phases. LC structures were optically analyzed using Nikon ECLIPSE E600 polarized microscope under polarizers in transmission mode, and the images were taken with the 20× imaging Canon EOS 550D camera. Treated glass cells were used for microscopy observations. Furthermore, high-resolution ac calorimetry was also used to probe the phase behaviour.[52,53] Calorimetric measurements were performed using a house-in-built setup at Jožef Stefan Institute, Ljubljana. This fully computerized, dual-mode setup operating in both ac and relaxation modes over a broad temperature range between 80 and 470 K was used.[54,55]

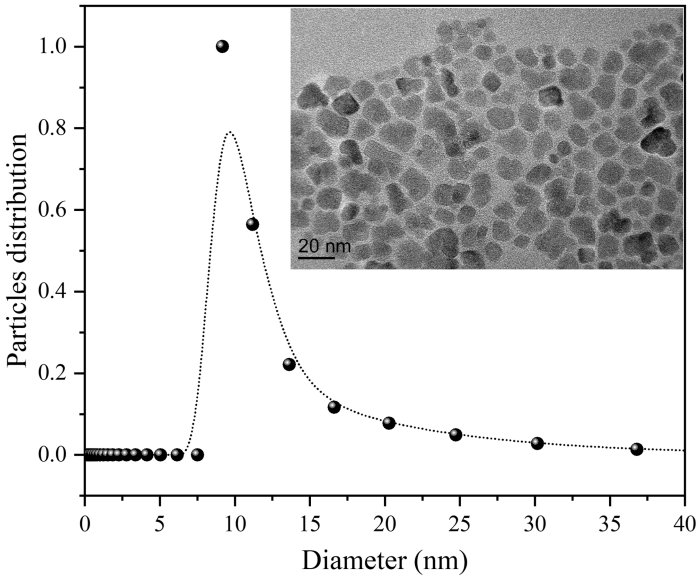

Fig. 1 DLS image of maghemite (γ-Fe_2O_3) magnetic nanoparticles. *X*-axis: NP's diameter and *Y*-axis: particle size probability distribution. The dotted line is the guide for the eye. TEM image of magnetic NPs is given in the inset.

3 Experimental Results

In the following, we present high-precision calorimetry and optical polarization measurements from which we extract the LC phase behavior. Measurements are carried out for bulk CE8 sample and three different CE8 – ferromagnetic NP mixtures: $\chi = 0.0001$, $\chi = 0.001$, and $\chi = 0.01$.

3.1 Heat Capacity Measurements

Figure 2 shows the temperature profiles of specific heat capacity $C_p(T)$ obtained from ac calorimetry in bulk and mixtures characterized by $\chi = 0.0001$, 0.001, and 0.01. The $C_p(T)$ measurements were obtained upon both cooling and heating from the I–N*–SmA phase with a scanning rate of 250 mK/h. The heat runs were conducted to confirm the phase sequence and the stability of the aforementioned phases upon heating and cooling. The $C_p(T)$ reference profile of pure CE8[26] is shown at the bottom layer. Measurements carried out in the mixtures do not yield clear evidence of the impact of NPs on BP configurations. Consequently, we determine the BP sequence using polarized optical microscopy (POM), described in the following subsection. The top two concentrations, $\chi = 0.001$ and 0.01, did not show visible confirmation of I-BP transition. In some cases, the isotropic to blue phase transitions are not visible due to the first-order transition character in CE8.[56] In mixtures with NPs, the first-order I-BP transition becomes sluggish and slightly smeared, resulting in a strongly suppressed I-BP peak measured in an ac calorimetric mode. The conventional ac calorimetric mode is mainly sensitive to the continuous part of enthalpy change and less to the latent heat of the I-BP transition.[56]

The bulk CE8 measurements[26] reveal a first-order phase transition from N*–SmA with a smaller shoulder at a low-temperature wing. The temperature profiles of $C_p(T)$ in Fig. 2 demonstrate that magnetic NPs have a relatively strong impact on TGB_A and N_L^* phase ordering. As NPs concentration increases, the transition peak shifts to higher temperatures and becomes broader. The presence of magnetic NPs introduces additional features along the N*–SmA phase transition. A clearly visible shoulder was created at a low-temperature wing of $C_p(T)$ data, representing the presence of the TGB_A and a small trace of N_L^* phase. The $C_p(T)$ peak of the $\chi = 0.0001$ mixture shows a slight widening; however, the aforementioned low-temperature anomaly is clearly visible for the $\chi = 0.001$ mixture. Furthermore, it becomes very pronounced for the $\chi = 0.01$ mixture, where the TGB_A phase is stabilized in a temperature range of ~3.0 K.

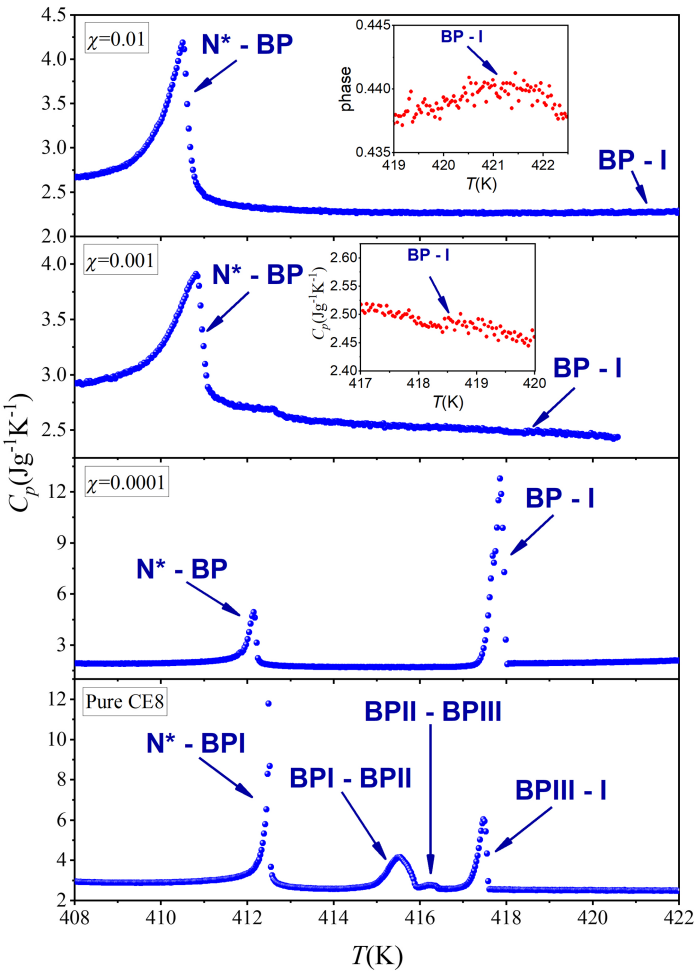

Fig. 2 The temperature dependence of specific heat $C_p(T)$ for pure CE8 (data taken from Ref. 26) and mixtures $\chi = 0.0001$, 0.001, and 0.01 magnetic NPs. Data points were obtained upon cooling with a scanning rate of 250 mK/h. Insets show suppressed I-BP anomalies. In the mixture with $\chi = 0.0001$, the I-BP anomaly was seen only in the phase of the heat capacity signal.

3.2 Optical Microscopy

Optical microscopy is used to take images upon cooling of the mixtures confined within planar cells. The temperature is slowly changed using an average scanning rate of 0.02 K/ min cooling to determine whether the phases are present in a given sample. Figure 3 shows the presence of the foggy blue phase, which is known as BPIII. The large-size platelets that appeared upon cooling are attributed to BPII. One observes the BPIII–BPII–BPI–N* transformation phase sequence upon cooling and slowly developing N* domains within BPI "sea." The evolution of BP textures on decreasing temperature is from left to right: BPIII, BPII, BPI, and stable N*. All of the textures remain stable when leaving the sample for longer at a fixed temperature.

Quantitative details are as follows. The BP temperature range widens slightly, from 5.0 K for pure CE8 to 5.9 K for $\chi = 0.0001$; 7.0 K for $\chi = 0.001$; and 6.9 K for $\chi = 0.01$. Therefore, for all concentrations, the total BP range is increased, and the transition temperature between I-BP is shifted to higher values: $\Delta T_{\text{I-BP}}$ (0.0001) = 0.9 K; $\Delta T_{\text{I-BP}}$ (0.001) = 2.0 K; and $\Delta T_{\text{I-BP}}$ (0.01) = 1.9 K, where $\Delta T_{\text{I-BP}}$ (χ) stands for the I-BP phase transition shift for a given χ with respect to pure CE8, respectively. The C_p phase transition peaks from BPIII–BPII and BPII–BPI observed in pure CE8 vanished in the presence of magnetic NPs. Only the $\chi = 0.001$ mixture exhibited a slight trace of BPI–BPII transition.

The optical textures are used to confirm the presence of the TGB_A and N_L^* phases in mixtures. In previous studies,[51,57] these textures were also stabilized by nonmagnetic NPs, such as Au NPs.[57] In magnetic NPs mixture with $\chi = 0.0001$, POM confirms the existence of N*,

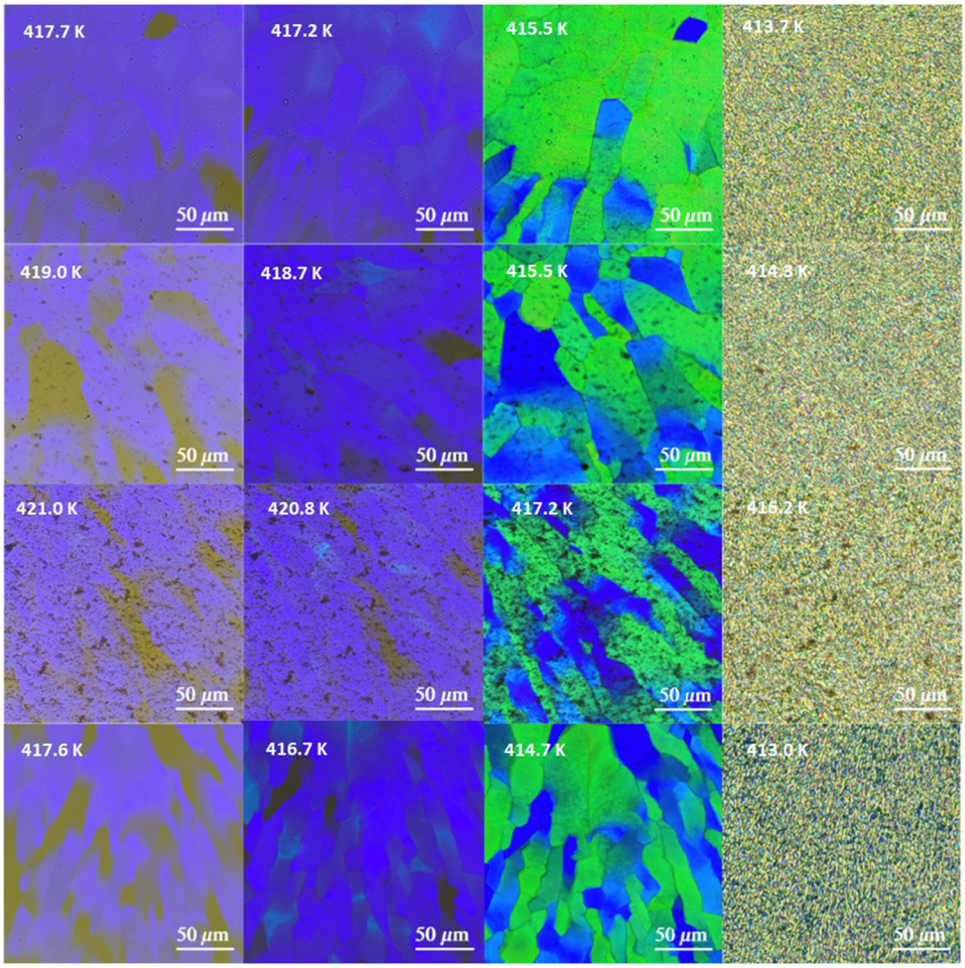

Fig. 3 Polarizing optical microscopy textures obtained on cooling for the (a) $\chi = 0.0001$, (b) $\chi = 0.001$, (c) $\chi = 0.01$ mixture, and (d) pure LC. The phase sequence from left to right is BPIII, BPII, BPI, and N* phase.

N_L^* and TGB_A textures upon cooling, as shown in Fig. 4. The intermediate textures corresponding to the TGB_A and N_L^* phases are stable with time when the temperature is constant. In agreement with calorimetric results, the POM textures confirm the increasing temperature window of TGB_A structures on increasing χ. The following POM textures can be explained by the continuous twisting of SmA slabs along the TGB_A helix, which appears rather metastable in bulk CE8, i.e., due to the proximity of the $TGB_A - N_L^* - N^*$ triple point. These textures are stable only in a narrow temperature range, which further shrinks with decreasing χ.

3.3 Phase Diagram

The temperature-concentration ($\chi - T$) phase diagram of mixtures of CE8 and magnetic NPs is depicted in Fig. 5. It was obtained by combining the results from optical microscopy and ac calorimetry, where we measured mixtures characterized by $\chi = 0.0001$, $\chi = 0.001$, and $\chi = 0.01$. The studied temperature window encompasses regimes where I, BPI, BPII, BPIII, N^*, N_L^*, TGB_A, and SmA phase could potentially appear.

We first discuss the sequence of BPs. As mentioned in Sec. 3.1, the heat capacity results failed to show the transition peak between I–BP phases (Fig. 2). However, we have visible confirmation from POM textures on the impact of χ on stability regimes of BPs (see Fig. 5). Our measurements clearly evidence the presence of the BPIII phase at relatively low χ values and vanishing of it on increasing χ. On the contrary, the temperature window of BPI is monotonously increasing. The solid circles represent the phase transition temperatures obtained by both POM and alternating current calorimetry (ACC) methods. The dotted lines indicate imaginary I–BP transition lines inspired by POM data.

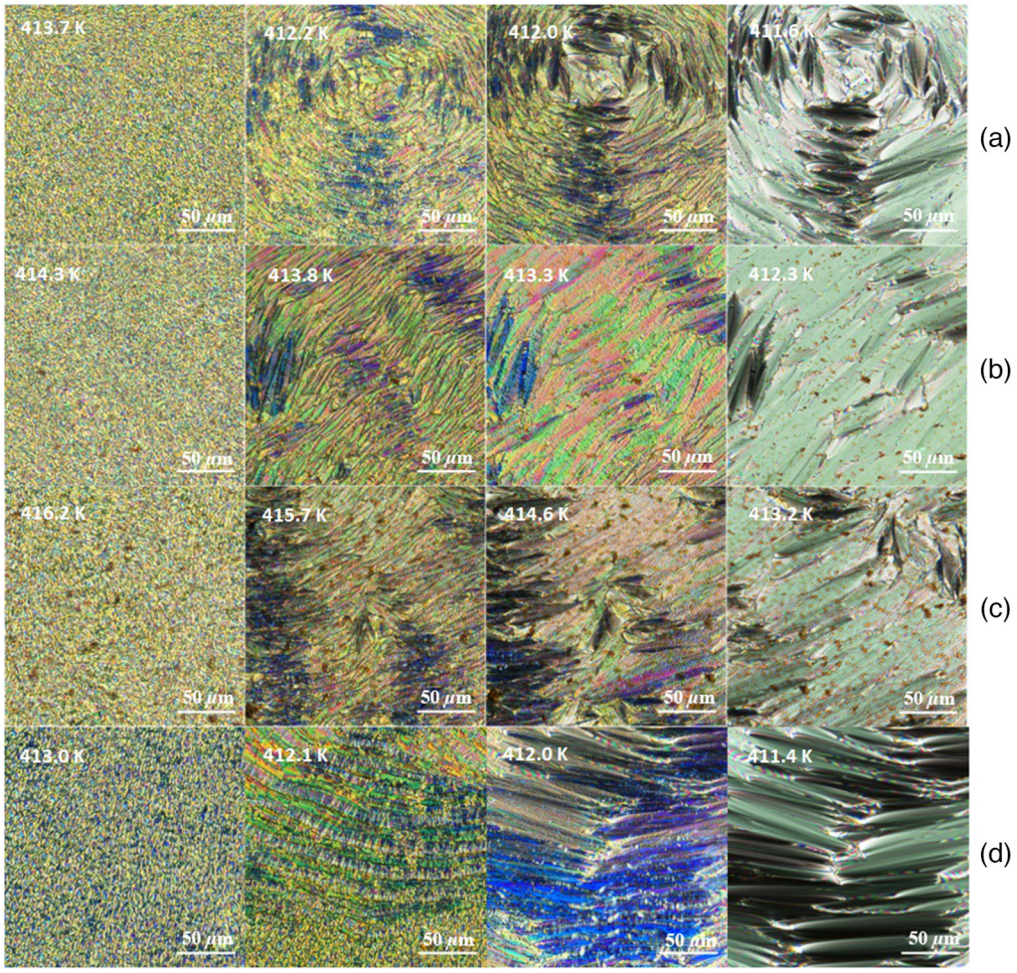

Fig. 4 Polarizing optical microscopy textures obtained on cooling for the (a) $\chi = 0.0001$, (b) $\chi = 0.001$, (c) $\chi = 0.01$ mixture, and (d) pure LC. The left-to-right phase sequence is as follows: N^*, N_L^*, TGB_A, and SmA phase.

Next, we focus on phases hosting screw dislocations (TGB_A and N_L^* phase). The dashed curves indicate $N_L^* - TGB_A$ and $TGB_A - SmA$ transition lines suggested by our measurements. One could clearly notice the significant rise in the stability range of the TGB_A and N_L^* phase. The latter phases could be metastable in pure bulk CE8 samples.[51,58] Note that these configurations could also be stabilized by nonmagnetic particles. For example, Trček et al.[58] observed a 3.4 K stability window in the CE8 + CdSSe $\chi = 0.05$ mixture. A similar temperature stability window was obtained for the CE8 + Au NPs $\chi = 0.02$ mixture.[58] In our case, we obtained similar results in even smaller concentrations of NPs (i.e., in $\chi = 0.001$ and $\chi = 0.01$ mixtures).

4 Discussion

A wider range of BPI and higher I-BPI phase transition temperatures have been observed. Despite the addition of magnetic NPs, the heat capacity anomaly of the I–BP transition remains sharp and similar to the pure CE8 for all reported concentrations. The transition temperatures between I–BPI remain rather close to the pure CE8 for low-concentration mixtures (i.e., $\chi = 0.0001$). This suggests that even a smaller concentration of magnetic NPs is sufficient to suppress the BPII range, acting similarly as in Refs. 26, 30, 47, 59, and 60.

The $\chi - T$ phase diagram of magnetic NPs mixtures shows a similarity to that of Au nanorods,[58,60] where the BPI phase extensively stabilized, and the BPIII phase is suppressed as increasing χ. It appears that used magnetic NPs efficiently stabilize only the BPI structure by magnetic NPs assembling at the cores of defects, like in the cases of Au nanorods and platelet NPs.[60]

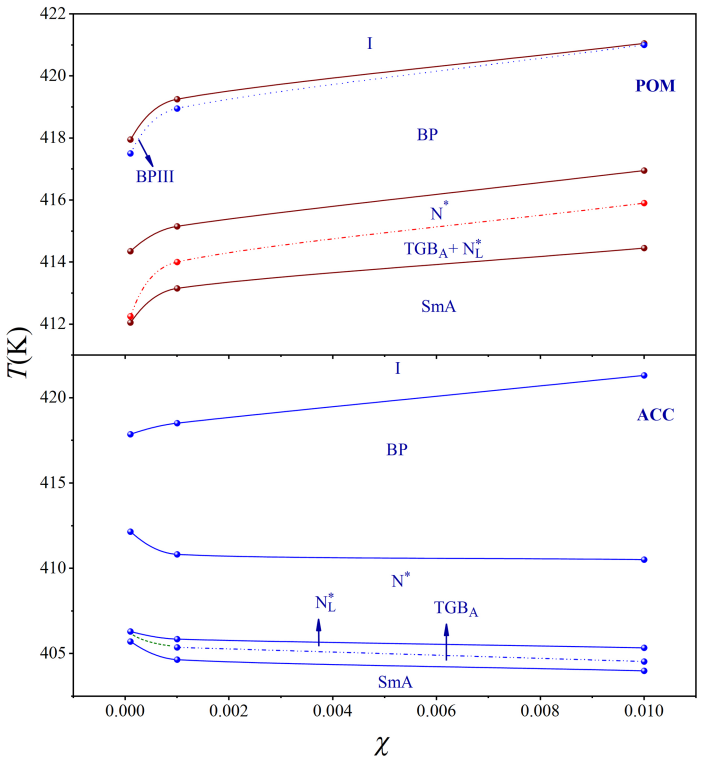

Fig. 5 The phase diagram of CE8 and CE8-magnetic NPs mixtures; (top) optical textures (POM) upon cooling and (bottom) heat capacity (ACC) data upon cooling. Note that heat capacity scans are performed at a much slower scanning rate. Therefore, POM results better reveal the quantitative sequence of nearly metastable phases.

Similar results were also observed in the case of anisotropic Au nanorods. In both cases (magnetic NPs and Au nanorods), only BPI was stabilized, while BPII and BPIII were suppressed. As in the case of NPs, platelets induce the nematic order and destroy isotropic symmetry due to their anisotropic nature. This suggests that the magnetic NPs stabilize the BPI with lower symmetry close to the nematic long-range order. In addition, magnetic NPs can form chains and act as rods, indicating the possible formation of anisotropic clusters of magnetic NPs in defect cores, mimicking the Au nanorods.

Concerning the I–BP transition temperature, as revealed by previous studies, the I–BP transition is slightly shifted towards lower temperature or stays the same for small spherical NPs. In the case of large spherical NPs, I–BP transition temperature is increased. In the case of magnetic NPs, which are of similar size as spherical Au NPs and Au nanorods, the $T_{\text{I-BP}}$ transition temperature is increased. The $T_{\text{I-BP}}$ transition shift is related to the interplay of several mechanisms. First, it appears that the same DCR mechanism is present in the mixture, which imposes the $T_{\text{I-BP}}$ increase. However, this is less efficient when a sample approaches the $T_{\text{I-BP}}$, where the correlation length attains its maximum value, and the volume occupied by defects is larger. Second, the elastic distortion induced by the NPs imposes the opposite tendency, i.e., decreases $T_{\text{I-BP}}$. Another elastic mechanism is a reduction of fluctuation of disclination lines due to the assembling of heavy NPs, such as spherical Au and large anisotropic NPs within the defect cores or their vicinity.

The results obtained by ac calorimetry demonstrate that the dispersion of magnetic NPs can moderately stabilize the short-range TGB_A order between the N^* and SmA phases of CE8. It is clearly seen that the presence of magnetic NPs gradually smears the N^*–SmA transition, and the visible shoulders are created while increasing the χ at the low-temperature wing, which represents TGB_A existence. For additional confirmation of the TGB_A presence, optical textures were taken with three given mixtures at specific temperature ranges. The higher concentrated mixtures $\chi = 0.01$ and $\chi = 0.001$ confirm the existence of an intermediate texture between the SmA and the oily streaks characteristic of the N^* phase.[57] Those intermediate textures were previously

observed in the cases of Au nanorods[58] and Au NPs[57] stabilized TGB_A phase. The following textures corresponding to the N_L^* and TGB_A phases are stable if the temperature is kept at a constant value. In agreement with calorimetric measurements, the POM textures confirm the stable TGB_A phase.

The magnetic NPs have a similar diameter to Au nanorods[58] and Au NPs,[57] which have also successfully stabilized the TGB_A phase. The heat capacity results are very similar to those of Au nanorods, i.e., anisotropic NPs. We conclude that the stabilization of TGB_A indicates that magnetic NPs form anisotropic clusters in defect cores, similar to Au nanorods. This indicates the possible anisotropic cluster formation of magnetic NPs in defect cores mimicking the Au nanorods.

5 Conclusions

Our finding enhances the list of material and geometrical NP properties that can be exploited to enhance specific ordered (BPI, BPII, and TGB_A) and disordered (BPIII, N_L^*) assemblies of line defects. Different configurations of TDs exhibit different effective symmetries that could be exploited for numerous applications, particularly in the electro-optic and photonic realms.

A detailed understanding of how various pathways could be exploited to nucleate and stabilize desired complex assemblies of TDs is of strong interest in fundamental science. Namely, the principal generic TDs creating mechanism are symmetry breaking phase transitions. These are commonly described by order parameter fields that consist of two qualitatively different components: the amplitude field and the phase field. TDs emerge due to the degeneracy of the order parameter phase field component. The degeneracy could give rise to frustrations in local phase ordering which could be resolved by introducing TDs. Their local stability is topologically protected, and topological features are independent of microscopic details. Note that topology is concerned with properties that are conserved in continuous field transformations. For this reason, gained knowledge in studying the stability of TDs in a particular physical system is in general, of cross-fertilizing utility, and could provide additional insight into the stability of TDs in other physical systems, spanning particle physics, condensed matter, and even cosmology.

Some of these universal features are also well manifested in our study. For example, disclinations (line defects in orientational order) and dislocations (line defects in translational order) exhibit qualitatively different defect core structures. In dislocations, the core is essentially biaxial. On the other hand, within dislocation cores, the smectic layer order is melted, while the accompanying orientational order could exhibit nematic uniaxial order. Nevertheless, the same NPs efficiently stabilize qualitatively different defect assemblies. The primary universal stabilization source is the reduction of condensed free energy penalty within defect cores. However, several studies reveal that curvature (in particular Gaussian curvature of a relevant physical field) might also play a significant role. A detailed understanding of this impact is still lacking, and additional experimental, numerical, and theoretical studies of this feature are needed.

Code, Data, and -Materials

The manuscript does not contain any proprietary code, data, or materials.

Acknowledgments

This work was part of A.G.'s PhD dissertation and supported by ADFUTURA, Public Scholarship, Development, Disability, and Maintenance Fund of the Republic of Slovenia and ARRS program (Grant No. P1-0125). We thank G. Cordoyiannis for useful discussions during this work. The authors have no potential conflicts of interest to disclose.

References

1. M. Kleman and O. Laverntovich, "Soft matter physics: an introduction," in *Partially Ordered Systems*, Springer New York, New York (2004).
2. J. P. Sethna, *Theory of the Blue Phases of Chiral Nematic Liquid Crystals*, pp. 305–324, Springer, New York (1987).
3. L. Navailles et al., "Structural study of a commensurate TGB-a phase and of a presumed chiral line liquid phase," *Phys. Rev. Lett.* **81**(19), 4168–4171 (1998).

4. Y. Hisakado et al., "Large electro-optic Kerr effect in polymer-stabilized liquid-crystalline blue phases," *Adv. Mater.* **17**(1), 96–98 (2005).
5. A. Gudimalla et al., "Nanoparticle-stabilized lattices of topological defects in liquid crystals," *Int. J. Thermophys.* **41**(4), 51 (2020).
6. S. Meiboom and M. Sammon, "Structure of the blue phase of a cholesteric liquid crystal," *Phys. Rev. Lett.* **44**(13), 882–885 (1980).
7. R. D. Kamien and T. C. Lubensky, "Twisted line liquids," *J. Phys. I* **3**(11), 2131–2138 (1993).
8. F. Reinitzer, "Beiträge zur kenntniss des cholesterins," *Monatsh. Chem.* **9**(1), 421–441 (1888).
9. H. J. Coles and M. N. Pivnenko, "Liquid crystal 'blue phases' with a wide temperature range," *Nature* **436**(7053), 997–1000 (2005).
10. I. Dierking et al., "Stabilising liquid crystalline blue phases," *Soft Matter.* **8**(16), 4355 (2012).
11. E. P. Koistinen and P. H. Keyes, "Light-scattering study of the structure of blue phase III," *Phys. Rev. Lett.* **74**(22), 4460–4463 (1995).
12. E. Dubois-violette, B. Pansu, and P. Pieranski, "Infinite periodic minimal surfaces: a model for blue phases," *Mol. Cryst. Liq. Cryst. Incorp. Nonlinear Opt.* **192**(1), 221–237 (1990).
13. J. Yan et al., "Polymer-stabilized optically isotropic liquid crystals for next-generation display and photonics applications," *J. Mater. Chem.* **21**(22), 7870 (2011).
14. W. Cao et al., "Lasing in a three-dimensional photonic crystal of the liquid crystal blue phase II," *Nat. Mater.* **1**(2), 111–113 (2002).
15. W. Zhang et al., "Blue phase liquid crystals affected by graphene oxide modified with aminoazobenzol group," *Liq. Cryst.* **43**(5), 573–580 (2016).
16. J. P. F. Lagerwall and G. Scalia, "A new era for liquid crystal research: applications of liquid crystals in soft matter nano-, bio- and microtechnology," *Curr. Appl Phys.* **12**(6), 1387–1412 (2012).
17. H. Iwamochi and A. Yoshizawa, "Electro-optical switching in blue phases induced using a binary system of a t-shaped nematic liquid crystal and a chiral compound," *Appl. Phys Express* **1**(11), 111801 (2008).
18. H.-Y. Liu et al., "Optically tunable blue phase photonic band gaps," *Appl. Phys. Lett.* **96**(12), 121103 (2010).
19. H. Kikuchi et al., "Polymer-stabilized liquid crystal blue phases," *Nat. Mater.* **1**(1), 64–68 (2002).
20. G. P. Alexander and J. M. Yeomans, "Stabilizing the blue phases," *Phys. Rev. E* **74**(6), 061706 (2006).
21. A. Yoshizawa et al., "The role of a liquid crystal oligomer in stabilizing blue phases," *Liq. Cryst.* **34**(9), 1039–1044 (2007).
22. H. Yoshida et al., "Nanoparticle-stabilized cholesteric blue phases," *Appl. Phys Express* **2**(12), 121501 (2009).
23. S. Taushanoff et al., "Stable amorphous blue phase of bent-core nematic liquid crystals doped with a chiral material," *J. Mater. Chem.* **20**(28), 5893 (2010).
24. K.-M. Chen et al., "Submillisecond gray-level response time of a polymer-stabilized blue-phase liquid crystal," *J. Disp. Technol.* **6**(2), 49–51 (2010).
25. G. Cordoyiannis et al., "Blue phase III widening in CE6-dispersed surface-functionalised CdSe nanoparticles," *Liq. Cryst.* **37**(11), 1419–1426 (2010).
26. B. Rožič et al., "Theoretical and experimental study of the nanoparticle-driven blue phase stabilisation," *Eur. Phys. J. E* **34**(2), 17 (2011).
27. H. Choi et al., "Polymer-stabilized supercooled blue phase," *Appl. Phys. Lett.* **101**(13), 131904 (2012).
28. L. Wang et al., "Hysteresis-free blue phase liquid-crystal-stabilized by ZnS nanoparticles," *Small* **8**(14), 2189–2193 (2012).
29. M. Lavrič et al., "The effect of graphene on liquid-crystalline blue phases," *Appl. Phys. Lett.* **103**(14), 143116 (2013).
30. M. Lavrič et al., "Effect of anisotropic MoS 2 nanoparticles on the blue phase range of a chiral liquid crystal," *Appl. Opt.* **52**(22), E47 (2013).
31. I. Gvozdovskyy, "'Blue phases' of highly chiral thermotropic liquid crystals with a wide range of near-room temperature," *Liq. Cryst.* **42**(10), 1391–1404 (2015).
32. M. A. Gharbi et al., "Reversible nanoparticle cubic lattices in blue phase liquid crystals," *ACS Nano* **10**(3), 3410–3415 (2016).
33. S.-Y. Jo et al., "Polymer stabilization of liquid-crystal blue phase II toward photonic crystals," *ACS Appl. Mater. Interfaces* **9**(10), 8941–8947 (2017).
34. F. Liu, G. Ma, and D. Zhao, "Nickel nanoparticle-stabilized room-temperature blue-phase liquid crystals," *Nanotechnology* **29**(28), 285703 (2018).
35. Y. Zhao et al., "Blue phase liquid crystals stabilized by graphene oxide modified with aminoalkyl group," *Mol. Cryst. Liq. Cryst.* **664**(1), 1–8 (2018).
36. P. G. de Gennes, "An analogy between superconductors and smectics A," *Solid State Commun.* **88**(11–12), 1039–1042 (1993).
37. S. R. Renn and T. C. Lubensky, "Abrikosov dislocation lattice in a model of the cholesteric–to–smectic-A transition," *Phys. Rev. A* **38**(4), 2132–2147 (1988).

38. L. Navailles et al., "Smectic a twist grain boundary phase in three new series with chiral (L) lactic acid derivatives," *Liq. Cryst.* **15**(4), 479–495 (1993).
39. L. Navailles, P. Barois, and H. T. Nguyen, "X-ray measurement of the twist grain boundary angle in the liquid crystal analog of the Abrikosov phase," *Phys. Rev. Lett.* **71**(4), 545–548 (1993).
40. J. W. Goodby et al., "A new molecular ordering in helical liquid crystals," *J. Am. Chem. Soc.* **111**(21), 8119–8125 (1989).
41. T. C. Lubensky and S. R. Renn, "Twist-grain-boundary phases near the nematic–smectic- a –smectic-C point in liquid crystals," *Phys. Rev. A* **41**(8), 4392–4401 (1990).
42. G. Srajer et al., "Structural measurements on the liquid-crystal analog of the Abrikosov phase," *Phys. Rev. Lett.* **64**(13), 1545–1548 (1990).
43. K. J. Ihn et al., "Observations of the liquid-crystal analog of the Abrikosov phase," *Science (1979)* **258**(5080), 275–278 (1992).
44. O. D. Lavrentovich et al., "Helical smectic A," *Europhys. Lett.* **13**(4), 313–318 (1990).
45. S. R. Renn and T. C. Lubensky, "Existence of a Sm-C grain boundary phase at the chiral MAC point," *Mol. Cryst. Liq. Cryst.* **209**(1), 349–355 (1991).
46. Z. Kutnjak et al., "Supercritical conversion of the third blue phase to the isotropic phase in a highly chiral liquid crystal," *Phys. Rev. Lett.* **74**(24), 4859–4862 (1995).
47. E. Karatairi et al., "Nanoparticle-induced widening of the temperature range of liquid-crystalline blue phases," *Phys. Rev. E* **81**(4), 041703 (2010).
48. S. Gyergyek et al., "Hydrothermal growth of iron oxide NPs with a uniform size distribution for magnetically induced hyperthermia: structural, colloidal and magnetic properties," *J. Alloys Comp.* **694**, 261–271 (2017).
49. C. Bahr and H. Kitzerow, "Chirality in liquid crystals," in *Partially Ordered Systems*, Springer-Verlag, New York (2001).
50. G. Cordoyiannis et al., "Different modulated structures of topological defects stabilized by adaptive targeting nanoparticles," *Soft Matter.* **9**(15), 3956 (2013).
51. M. Trček et al., "Twist-grain-boundary-A* phase stabilisation in confined geometry by the interfaces," *Liq. Cryst.* **43**(10), 1437–1447 (2016).
52. C. W. Garland, "Calorimetric studies," in *Liquid Crystals: Experimental Study of Physical Properties and Phase Transitions*, S. Kumar, Ed., p. 240, Cambridge University Press (2001).
53. H. Yao, K. Ema, and C. W. Garland, "Nonadiabatic scanning calorimeter," *Rev. Sci. Instrum.* **69**(1), 172–178 (1998).
54. Z. Kutnjak, "Ferroelectric smectic-C* liquid-crystal phase: reexamination of the electric-field influence," *Phys. Rev. E* **70**(6), 061704 (2004).
55. Z. Kutnjak, J. Petzelt, and R. Blinc, "The giant electromechanical response in ferroelectric relaxors as a critical phenomenon," *Nature* **441**(7096), 956–959 (2006).
56. G. Cordoyiannis et al., "Quantum dot-driven stabilization of liquid-crystalline blue phases," *Front. Phys.* **8**, 315 (2020).
57. M. Trček et al., "Twist-grain boundary phase induced by Au nanoparticles in a chiral liquid crystal host," *Liq. Cryst.* **44**(10), 1575–1581 (2017).
58. M. Trček, "Nanoparticle-induced twist grain boundary phases and electrocaloric effect in liquid crystals," PhD thesis (2017).
59. M. Lavrič et al., "Blue phase range widening induced by laponite nanoplatelets in the chiral liquid crystal CE8," *Mol. Cryst. Liq. Cryst.* **615**(1), 14–18 (2015).
60. M. Lavrič, "Stabilization of cholesteric blue phases by nanoparticles and nematic caloric effects induced by external fields," Doctoral Thesis (2018).

Biographies of the authors are not available.